Materials Today: Proceedings xxx (xxxx) xxx

Contents lists available at ScienceDirect

Materials Today: Proceedings

journal homepage: www.elsevier.com/locate/matpr

Ni based tungsten heavy alloy processed by PBF-L additive manufacturing and conventional LPS routes

F. Miranda [a,*], M.O. dos Santos [b], D. Rodrigues [c], R.S. Coelho [d], G.F. Batalha [a]

[a] University of São Paulo, Polytechnic School, EPUSP – PMR, São Paulo, Brazil
[b] Mauá Institute of Technology, University Centre, São Caetano do Sul, Brazil
[c] BRATS Sintered Filters and Metallic Powders, Cajamar, Brazil
[d] SENAI CIMATEC - Institute of Innovation for Forming & Joining of Materials, Salvador, Bahia, Brazil

ARTICLE INFO

Article history:
Available online xxxx

Keywords:
W-Ni
Additive manufacturing
PBF-L
Liquid phase sintering
Microstructure
Mechanical properties

ABSTRACT

Tungsten Heavy alloys (WHA's) have attracted attention in different industrial areas, such as biomedical and military devices, in the application of shielding for ionizing radiation. In this study, samples of W-30Ni alloy were additively fabricated by the laser beam selective Powder Bed Fusion-Laser (PBF-L) techniques, and compared with the conventional route, liquid phase sintering (LPS). The samples were prepared by mass balance, compacted from 50 to 125 MPa, without polymeric binders, and vacuum sintered at temperatures of 1330, 1370 and 1420 °C. For the PBF-L technique, a vibrating device made it possible to improve the fluidity of the W-Ni mixture, which has low sphericity, low fluidity and at the same time the compressibility of the mixture, promoted through a roller compactor. The thin deposition layers of the powder mixture were applied evenly and well distributed in the powder bed to avoid defects and cracks during sintering. The parameters of the PBF-L process varied with power from 50 to 125 W and scanning speed laser from 25 to 120 mm/s. The different microstructures, obtained by Optical Microscopy (OM) and Scanning Electron Microscope (SEM), and properties were compared with the two sintering techniques, direct (PBF-L) and indirect (LPS). The microhardness of the PBF-L samples was higher than those processed by the LPS technique.

Selection and peer-review under responsibility of the scientific committee of the 16th Global Congress on Manufacturing and Management 2022.

1. Introduction

Tungsten-based heavy metal parts use to be manufactured by powder metallurgy (PM), or sintered technology, by Powder Extrusion Molding (PEM) and Powder Injection Molding (PIM). Additive manufacturing (AM), Powder Bed Fusion (PBF) technique in metals, may be an alternative manufacturing process for high melting point refractory metals [1]. Tungsten (W) Heavy Alloys (WHA's) are tungsten pseudo-alloys with a nickel (Ni), iron (Fe) and copper (Cu) binding phase, fabricated by the sintering process, by liquid Ni phase on the surface of the W particles; stands out because of particular properties due to its high melting point and density, excellent thermal conductivity, low thermal expansion and have application in aerospace, military, electronics and marine industries, plasma coated shields in nuclear industry for shielding, counterweights, kinetic energy penetrators, heat sinks for electronics and vibrating masses for cell phones [2–4]. The main advantage of Ni/Fe based WHA's is their ability to be machined into complex geometries using conventional cutting tools; The hardness of these WHA's under most conditions is only 30 HRC or just under 28 HRC, it can be easily machined [5]. One of the advantages of the AM, PBF-L technique, is the ability to manufacturing tungsten components in complex and complicated shapes with small dimensions, something that cannot be easily manufactured by traditional techniques such as casting, forging, machining and conventional powder metallurgy; and has been used more frequently by various industrial sectors to reduce production steps and costs, mainly for the manufacture of high-value, low-volume mechanical components and for complex shapes [6]. W-based materials present several difficulties in the AM, PBF-L technique in metals, due to the high melting temperature, high thermal conductivity, high viscosity and for rapid cooling, in the cold substrate, undesirable

* Corresponding author at: University of São Paulo, Polytechnic School, EPUSP – PMR, São Paulo, Brazil.
E-mail address: fabio.miranda@usp.br (F. Miranda).

https://doi.org/10.1016/j.matpr.2023.05.567
2214-7853/
Selection and peer-review under responsibility of the scientific committee of the 16th Global Congress on Manufacturing and Management 2022.

effects such as ball formation and oxidation tendencies may occur. Understanding powder type, as critical material, and process parameters (laser power, distance between laser scan tracks, layer thickness, scan speed), affect PBF-L processing for WHA's [7]. This work aims to compare the characterization and processing of the W-30Ni alloy for the two techniques, conventional LPS and PBF-L additive manufacturing, systematically using the relationships between process variables and the quality of the samples produced.

2. Materials and experimental methodology

2.1. Preparation of W-30Ni alloy

The following metallic powders were used in this work, as shown in Table 1.

The tungsten powder, Fig. 1(A) shows, Scanning Electron Microscope (SEM), a granulometric distribution smaller than 2 μm and the particles have spherical and irregular polygonal shapes. The nickel carbonyl powder, Fig. 1 (B), has particles with dendritic and porous shapes, with dimensions smaller than 15 μm. The 70 W-30Ni alloy mixture was prepared using the conventional powder metallurgy technique (mixing, drying, compaction, sintering, sample rectification and subsequent analysis). In Fig. 1(C) the Backscattered Electron Imaging (BEI) of the W-30Ni mixture is compared with the secondary electron imaging (SEI) to identify Ni, darker particles (8.9 g/cm^3) and W, lighter particles (19.2 g/cm^3).

2.2. Liquid phase sintering technique (LPS)

These W and Ni metal powders, according to Table 1, were mixed and homogenized by a conventional palette mixer, 3000 rpm, Fig. 2(A), for 3 h, using isopropyl alcohol as a lubricant. The high energy Attritor mill was not used, nor was grinding to avoid the reduction and crushing of the metallic tungsten and nickel grains. After the mixing step, the isopropyl alcohol was removed by means of conventional drying in an oven at a temperature of 200 °C for 2 h. Compaction was carried out in the dry uniaxial direction, that is, without polymeric binders, in a metallic matrix with a rectangular section of 12 × 37 mm, Fig. 2(B). The compression pressure used ranged from 50 to 125 MPa.

The green compacted samples, Fig. 2(C), were finally sintered in a vacuum furnace, Fig. 2 (D), with temperatures varying from 1330, 1370 and 1420 °C, heated for 3 h, stabilized for 60 min, for all samples, and slow cooled, inside the vacuum furnace, Fig. 2 (B). The result of the physical behavior, in particular the density, of a W-Ni alloy, can be obtained by the expression (1).

$$\rho_t = \left[\frac{\rho_{Ni}.\rho_W}{\rho_W \, x\,(Ni\%) + \rho_{Ni}\, x\,(W\%)}\right].100\% \quad (1)$$

where ρt: theoretical density of the binary W-Ni alloy; Ni%: mass percentage of Ni; W%: mass percentage of W; Tungsten density (ρ_W) equivalent to 19.2 g/cm^3; Nickel density (ρ_{Ni}) equivalent to 8.9 g/cm^3. According to the mixing rule, by mass balance, 70% W and 30% Ni, by weight, the theoretical density of 14.25 g/cm^3, via expression (1).

2.3. Direct sintering techniques via powder bed fusion - laser (PBF-L)

The direct sintering process, PBF-L, eliminates the steps of grinding, drying, sieving, paraffin binding, pre-sintering in hydrogen furnaces, green machining, when compared to the conventional process of the LPS fabrication route. The compaction of the metallic powders was carried out in the Omnisint-160 model machine, Fig. 3 (A), performed by a vibrating device with a metal roller, Fig. 3 (B), whose rotational speed is controlled independently of its displacement speed. Compared to the conventional compaction process of green parts using a metal matrix, the cross section of the powder bed in the direct sintering system is much longer, Fig. 3 (C), therefore it is difficult or almost impossible to provide the powder bed with high pressure when compared to the LPS technique. For this, a compressor roller was developed and coupled to the powder fluidized device, Fig. 3 (D), to spread the powder through its translation and rotation movement that can compress at the same time. Compaction of thin layers with a roller is interesting for metallic powder materials for applications that focus only on additive manufacturing application [7]. In this operation, the metallic powder flows under the fluidizing container, which at the same time is spread and compacted, Fig. 4 (A).

Regarding the investigation of the PBF-L process parameters, Fig. 3 (D), the tracks are created using multiple laser powers as a function of the scan speed. According to the scanning system of the OmniSinter-160 equipment, from the company Omnitek Technology (Brazil), the scanning speed was varied from 50 to 150 mm/s, changing the laser exposure time (P_L = 500 W – 100%) while keeping the exposure point distance (Hs = 80 μm) of the laser at its minimum height value (Iz = 30 μm), focal diameter Laser 140 μm. The volumetric energy density applied to the samples can be calculated through the expression (2) [6,8]. Where: E_V (J/mm^3) is the energy density that relates Laser Power (P_L) to scan speed (v_S), distance between tracks (h_S) and layer thickness (I_Z).

$$E_V = \frac{P_L}{v_s.h_s.I_z} \quad (2)$$

In the sintering process, PBF-L, a continuous flow of argon was added, 0.3 litters per minute. Oxygen was present within the system, which ranged from 250 to 350 ppm. Samples were initially programmed to be produced with a height of 1020 μm (34 deposition layers). The thickness of the "I_z" layer used was kept fixed at 0.03 mm. Fig. 4(A) shows the illustration of the process parameters in PBF-L, compaction, scanning strategy and Fig. 4 (D) shows the schematic diagram of the adopted scanning strategy. As can be seen in Fig. 4 (B), a zigzag scan strategy was used for a single layer, with 65° rotation between adjacent layers, Fig. 4 (C). A compaction factor (Fc), calculated through the expression (3) [9], was defined for the roller compactor that passes through the powder bed for compressibility of metallic powder, while the roller rotates in a certain clockwise direction:

$$F_C = \frac{d_L}{d_s}$$

The compaction factor, for this device, indicates how much the powder bed layer (d_S) has retracted in relation to the initial layer (dL). More specifically, the layer-by-layer deposition process should follow the scheme shown in Fig. 4 (A) and (B).

Table 1
Properties of tungsten (W) and nickel (Ni) metallic powders.

Powder	Average Grain Size (μm)	Apparent Density (g/cm^3)	Degree of purity (%)	Manufacturing Route
Tungsten (W)	1.5	7.1	99.530	Hydrometallurgy and reduction by H_2
Nickel (Ni)	5.0	3.5	99.847	Carbonyl gas refining process

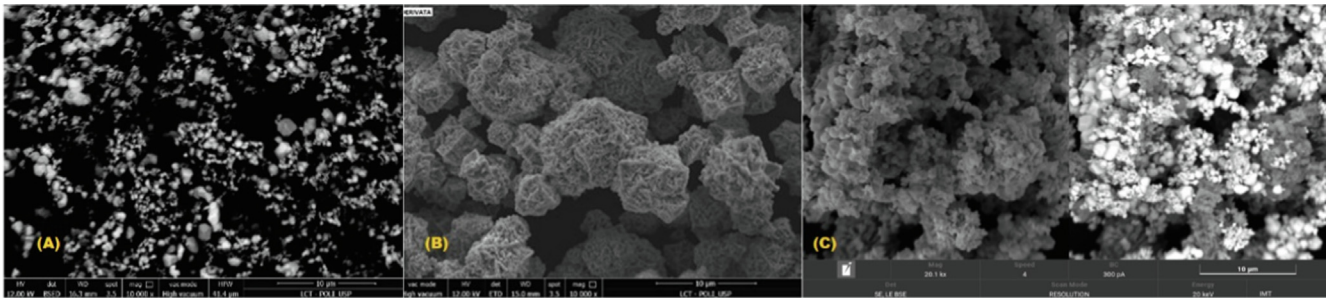

Fig. 1. (A) SEM of W metal powder; (B) SEM of Ni carbonyl powder and (C) BEI and SEI, are detected using SEM of the mixture of metallic powders in the proportion 70W:30Ni, by weight, highlighting the light powders for W, and the Ni powders, dark colors.

Fig. 2. (A) Conventional stirrer with a capacity of 3 kg of mixtures. (B) Compaction of specimens. (C) Rectangular samples of green compactsfor the LPS process. (D) Vacuum sintering furnace; (E) sintering thermal cycle. (For interpretation of the references to colour in this figure legend, the reader is referred to the web version of this article.)

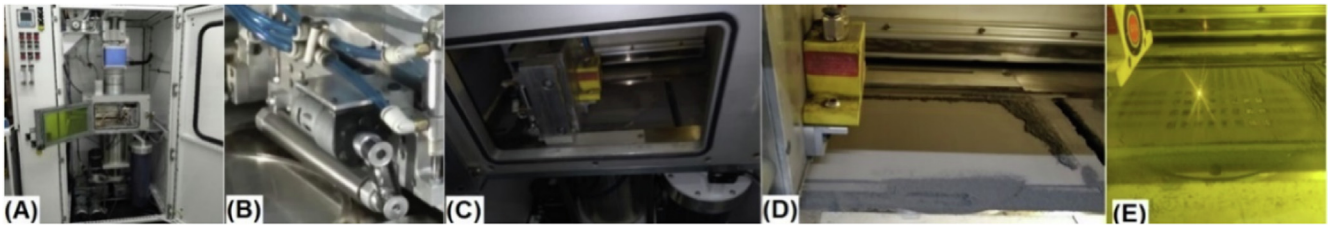

Fig. 3. (A) OmniSint-160 machine; (B) Vibration device with roller; (C) Sintering chamber; (D) powder bed flowability & compressibility; (E) Sintering with different parameter levels PL(W)x vs(mm/s).

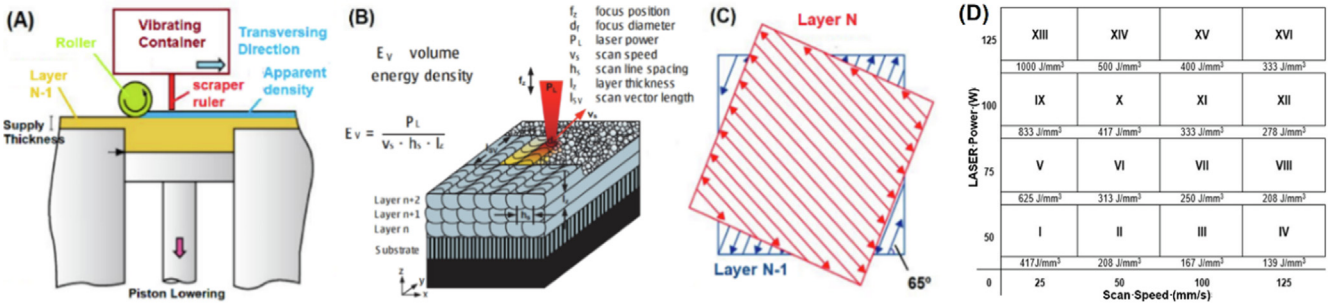

Fig. 4. (A) Compacting Method [9], (B) zig zag scanning strategy [8], (C) monolayer deposition strategy with 65° rotation and [10], (D) Sintering strategy via PBF-L - generated by distinct levels of factors (PL × vs).

Without the roller compactor and with the scraper ruler for spreadability of the W-Ni mixture in the powder bed, craters appear on the powder surface, Fig. 4 (A). With the roller compactor, fill in the gaps created by the scraper ruler and make the deposition layer uniform and even. In addition, it improves densification, going from a bulk density condition to a beaten and pressed or compacted density, as shown in Fig. 3 (D).

3. Results and discussions

After fabrication, via LPS and PBF-L, the samples were embedded in Bakelite and the surfaces were sanded with a diamond disk, in a polisher to remove the rough surface and then polished, in a polisher with nylon felt, in suspension of diamond powder based on of solid Vaseline, varying in the order of decreasing from 15 to 1 μm until the final polishing, for analysis of the apparent porosities. For the analysis of the microstructures in the OM and SEM, the electrolytic chemical attack was necessary, due to the

high corrosion resistance of Ni and W; with 3–6 Volts, for 3–5 s with a liquid reagent containing 10 g of NaOH dissolved in 100 cm^3 of distilled water. The sintered density tests were performed, Fig. 5(A); relative density (%), Fig. 5(B); Linear contraction (%), Fig. 5(C); volumetric contraction (%), Fig. 5(D); Vickers hardness (HV 1), Fig. 5(E); and Rockwell Hardness (HRC), Fig. 5(F), respectively.

The apparent porosity and microstructure analyze of the samples obtained by the LPS technique at temperatures of 1330, 1370 and 1420 °C are shown in Fig. 6(A). (B) and (C). Nickel pool phase, lack of spreadability around the W grains, with plenty of micro porosity points, evidencing a heterogeneous structure, due to the lack of wettability and spreadability of Ni in the W grains, this mechanism compromises the performance of the product, such as low densification, hardness, and other properties, therefore, should be avoided. WHA's have an average hardness of $HV_{0.5}$ 302 ± 10, which can be reduced with the presence of excessive porosity [10].

The theoretical densities for the binary composite W and Ni are respectively: 19.20 g/cm^3 and 8.91 g/cm^3, therefore, the theoretical density of the W-30Ni alloy is 14.25 g/cm^3. Metal powders from W-based alloys, are subjected to a compaction pressure of up to 200 MPa; and the sintering process takes place in two stages, consisting of primary solid–solid sintering and secondary sintering, solid–liquid phase. Solid state sintering temperatures can range from 1300 to 1450 °C, and in a hydrogen atmosphere [4]. In the conventional LPS technique, during sintering, the solid–solid bond between the metallic powders occurs, giving compact rigidity, before the emergence of the liquid phase (Ni), forming necks between the particles and porosities, the low wettability of Ni is perceived around the W [3]. Full density can be achieved in solid–solid and solid–liquid states, but the microstructures will not be spheroidized and the mechanical properties will be very low. Those containing tungsten content ranging from 60 to 90 % by weight, rich in Ni, are easily deformed, have high ductility and good machinability, making it possible to machine with inserts or conventional carbide cutting tools. WHA alloys (10% wt nickel metal binder phase) have many applications, one being as a balance weight in aircrafts. For this application, the pieces have a complex shape and must have the highest possible density, that is, less binder. However, it is a component that undergoes intense wear, and larger amounts of binder can provide less mass loss during operation. Furthermore, in the PBF-L process, the use of higher concentrations of binder can make the process viable, when compared to the process by liquid phase sintering, without the use of polymeric or paraffinic binders.

The main phase of these binary alloys is tungsten (CCC structure) and the mechanical properties must be very close to that of pure tungsten, example for average hardness values of 29 HRC (~290 HV or 64.0 HRA), for a heavy alloy WHA - *Densalloy* SD170, with a maximum of 32 HRC (~320 HV or 66.5 HRA) [5]**.** The same mixture of W-30 Ni powder applied in the LPS technique, was submitted to the PBF-L technique, in the OmniSint 160 equipment. Using laser powers, 50, 75, 100 and 125 W, in the OmniSint 160 machine, the samples manufactured by the PBF-L resulted in 34 layers (1020 μm) and with an average thickness of 649 ± 116 μm, which represents an average height shrinkage factor of 63.63% with a standard deviation of ± 36 %. The microstructure investigations involved creating a process map (LASER power versus Scan speed) resulting in various levels of volumetric energy density factors.

For the conventional press and sintering processes, the linear/volumetric shrinkage is influenced by the sintering temperature and by the green density (compaction pressure). The higher the sintering temperature or the lower the compaction pressure, the large will be the shrinkage. The sintering mechanisms via LPS, swelling can occur and swelling effects on the final sintering depends on the strength of the pressed body during sintering. The Fig. 5(G) and 5(H) shows that the swelling at 1420 °C, when the liquid has greater fluidity, does not occur only for samples compacted with 125 MPa, which have greater strength.

Fig. 7 (A) and (B) show, respectively, the apparent porosity and optical micrograph characteristics of the W-30Ni alloy, of the fusion results of a single track, distance from the exposure point (H_S = 80 μm) of the LASER at its minimum height value (I_Z = 30 μm), focal diameter Laser 140 μm. The strategy for the manufacture

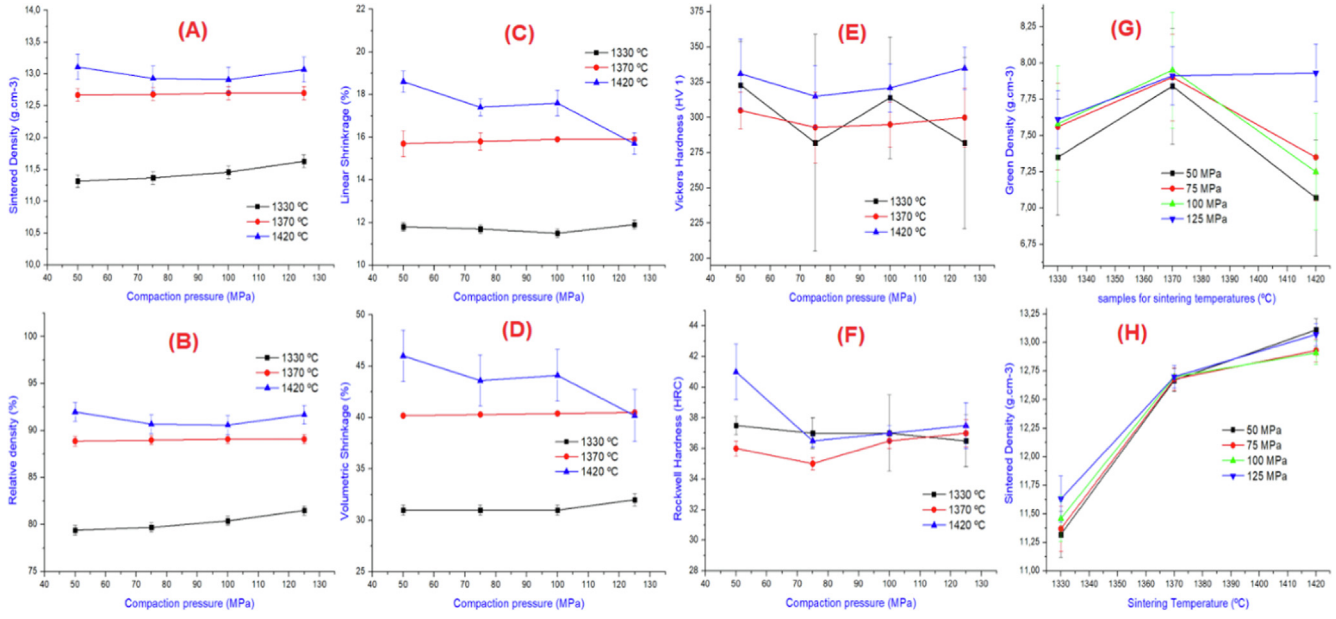

Fig. 5. (A) Properties of W-30Ni alloy samples produced in the LPS process, according to the compaction pressure, vacuum sintered at 1330 °C, 1370 °C and 1420 °C. (A) Sintered Density, (B) Relative density, (C) Linear Shrinkage, (D) Volumetric Shrinkage, (E) Vickers Hardness (HV1), (F) Rockwell Hardness, (G) Green Density and (H) The influence of sintering temperature in relation to the compaction pressure of the samples. (For interpretation of the references to colour in this figure legend, the reader is referred to the web version of this article.)

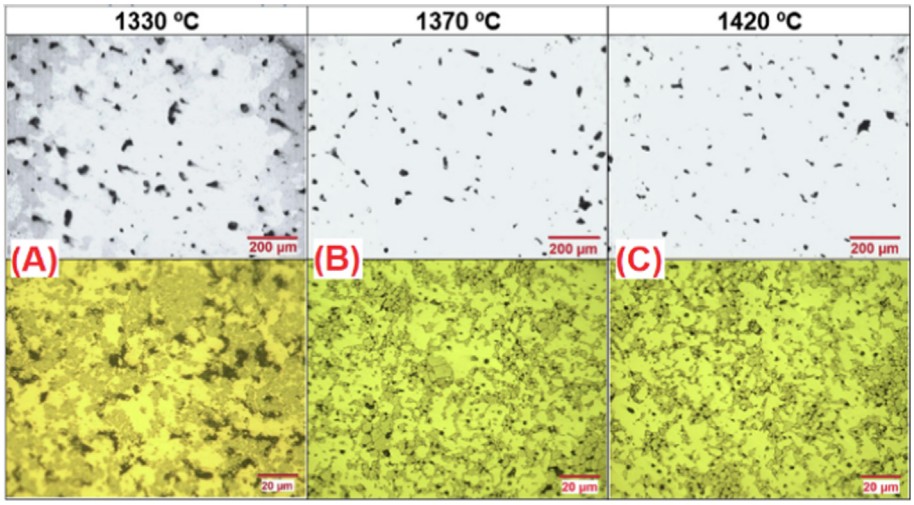

Fig. 6. Apparent porosity (OM 100x) and Microstructures (OM 1000x) of W-30Ni samples (125 MPa) produced in the LPS process, conventional route: (A) vacuum sintered at 1330 °C, (B) 1370 °C and (C) 1420 °C.

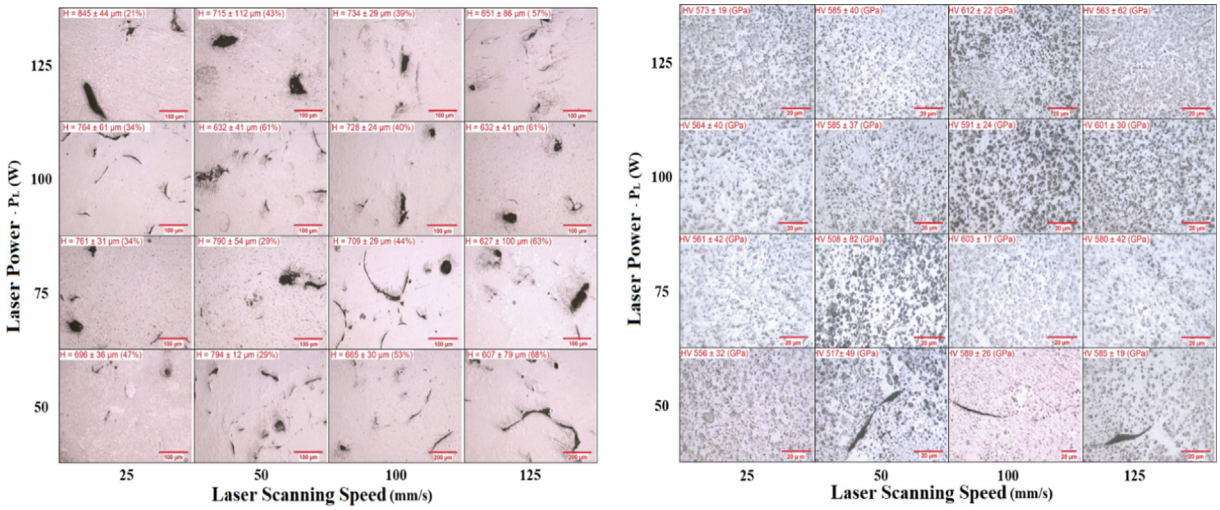

Fig. 7. (A) Porosity characteristics of W-Ni samples after distinct levels of volumetric energy density, with their respective final heights and compaction factor (Fc%) and (B) Characteristics of microstructures and grain size of W-Ni samples after various levels of volumetric energy density, with their microhardness at HV (1.0 kgf).

of mechanical parts and components, via PBF-L aiming at high density depends on a map or parameters of laser deposition energy density, it is recommended the minimum typical power of 200 W is used to melt the *WHA's* metallic powder that is in bed, on a metal table, preferably of the same alloy, using data from a parameterized 3D CAD file that will be sliced layer by layer, with a layer thickness in the range of 0.03–0.05 mm [6]. However, in this work, due to the high content of the nickel ligand phase, the powers from 50 to 125 W were taken into account in a bed of ANSI 1020 carbon steel.

The idea of working with low flowability tungsten and nickel mixtures was due to the difficulties in obtaining fine and spherical powders (higher flowability), especially considering W powders. PBF-L processes demand such characteristics; however, the use of high binder concentrations can compensate the poor flowability and packing, due to a high-volume fraction of liquid during the process. Li et al. [18], studied the refractory alloy of 90W-10(Ni, Fe), with spherical powders, for different combinations of process parameters by the PBF-L technique and the samples almost reached a total densification of 99% (relative density) and the Laser power had a relevant influence on the process, with a volumetric energy density (VED), value of 300 J/mm^3. The micro indentation hardnesses were higher than $HV_{0.3}$ 400. Vickers Hardness values, $HV_{1.0}$ (GPa), with their respective standard deviations, were calculated according to ASTM C1327-15 Standard Test Method for Vickers Indentation Hardness of Advanced Ceramics, expression (4), where "P" (kgf) is a force applied to the surface of the sample and "d" (mm) is the average length of the two diagonals of the indentation.

$$HV_P\,(\mathrm{GPa}) = 1,8544.\left(\frac{P}{d^2}\right) \tag{4}$$

It can be seen in Fig. 8, that with the increase in the volumetric energy density, for a single scanning speed of the LASER beam, it is accompanied by an increase in volume and a decrease in the viscosity of the Ni ligand matrix; due to hydrodynamics driven by the Marangoni effect, which becomes important for the distribution of W in the molten pool. However, if the scanning speed is increased, the heat-affected zone becomes larger, evidencing the lack of W fusion and obtaining a heterogeneous structure, Fig. 8 (B) and 9 (B), solution reprecipitation is favored with increasing energy, being the most important means to reach full density dur-

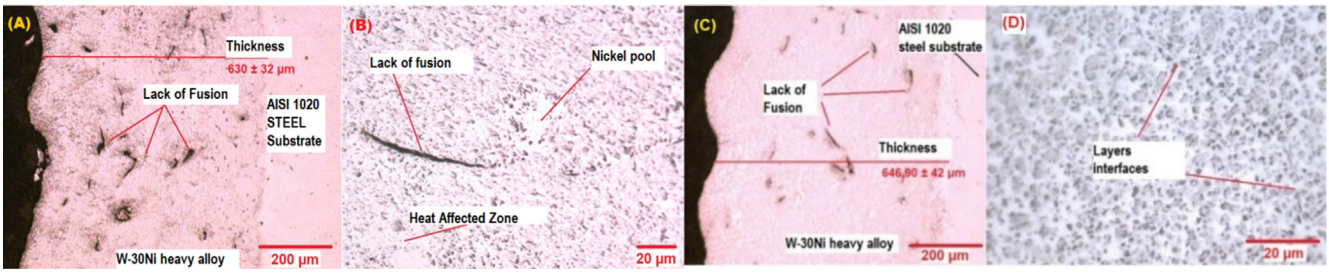

Fig. 8. (A) Total thickness of W-30Ni samples PBF-L; (B). Layer-to-layer, non-homogeneous, HAZ deposition interface sample III alloy; P_L = 50 W, vs = 100 mm/s and Ev = 167 J/mm^3, (C) Total thickness of sample VII by PBF-L; and (D). Layer-to-layer deposition interface, homogeneous structure, P_L = 75 W, vs = 100 mm/s and Ev = 250 J/mm^3.

ing liquid phase sintering [11]. It should be noted that in the contraction, the surface does not appear uniformly in any of the samples III and VII, respectively, Figs. 8 (A) and 9 (A). The width, length, amount of shrinkage and placement will vary depending on the associated process parameter values. In most samples, the contraction observed via OM increases as the scanning speed increases, this undesired effect favors the formation of porosity and the lack of fusion between the deposition layers.

The fabrication of tungsten samples by the PBF-L technique (SLM) is considered difficult due to the high melting point, high thermal conductivity, high viscosity and sensitivity to oxidation [6]. By using a laser, for high deposition energy densities, with oxygen levels below 320 ppm in the sintering chamber, complex geometries construction, even of refractory metals such as pure tungsten, can be realized. However, due to its intrinsic properties of high melting point, good thermal conductivity, high ductile to brittle transition temperature and high surface tension, sintering tungsten heavy metal and its alloys is a challenging task, resulting in parts, mainly, with cracked and/or porous microstructures. These unwanted defects such as apparent porosities, lack of fusion and microcracks seem to be inevitable for the PBF-L technique, no matter what process parameter was chosen, due to the high thermal stresses that tend to form in rapid melting and rapid solidification. Effective methods of reducing or eliminating these defects need to be investigated in the future [10]. In Fig. 9 (A) and 9 (B), presents the schematic curves of surface tension variation with temperature in a liquid metal. The penetration profile and the oscillations in the weld pool can be explained through the Marangoni convection mechanism. Curve (a) represents a high purity material ($dg/dT < 0$) and curve (b) a material contaminated with a surface-active element ($dg/d_T > 0$) [12]. The presence of oxygen can affect the surface tension of the weld pool and reverse the direction of the *Marangoni* flow, increasing the balling effect [1].

The intensity of thermocapillary convection can be characterized by the Marangoni number (Ma) defined as, expression (5):

$$M_a = \frac{d_\gamma}{dT}\frac{dT}{d_x}\frac{L^2}{\alpha.\eta} \tag{5}$$

where γ is the surface tension, $\frac{dT}{dx}$ is the temperature, is the thermal gradient, α is the thermal diffusivity and η is the viscosity of the liquid. Higher *Ma* numbers, Eq. (4), means strong circulation of molten metal and result in larger molten pools at the interface, compared to Fig. 9 (B) and 9 (D). It also means that the convective flow of the molten metal within the pool, driven by the surface tension gradient and with a higher Marangoni number, also results in a larger pool with high ratio, which helps to ensure proper bonding between the layers, therefore, lower porosity in the alloy [13]. The surface tension (γ) of the liquid metal decreases with increasing temperature, that is, $\frac{d_\gamma}{dT} < 0$; the hotter liquid metal with a lower surface tension at point "a" is pulled out through the cooler liquid metal with a higher surface tension at point "b"; that is, an outward shear stress is induced on the surface of the weld pool by the surface stress gradient along the surface of the pool [12], as shown in Fig. 9 (C). This causes the liquid metal to flow from the center of the surface to the edge of the pool and back below the surface of the pool, as shown in Fig. 9 (B), resulting some faults shown in Fig. 9 (E). The W-Ni phase diagram [14]; in Fig. 11, is especially important in the identification of solubility parameters and in the identification of the possible phases that can form during solidification, characterized by three intermediate phases, but there are several limitations [15].

For the chemical composition 70%W (BCC) and 30% Ni (FCC), there is predictability of forming the NiW phase, composition of 75.8% W, by mass. However, in non-homogeneous regions, with 44% W, by mass, the compound Ni_4W and the compound NiW_2 (with 86.3%W) can be formed, as shown in Fig. 10 (A), regarding that its formation is extremely sensitive to the presence of oxygen

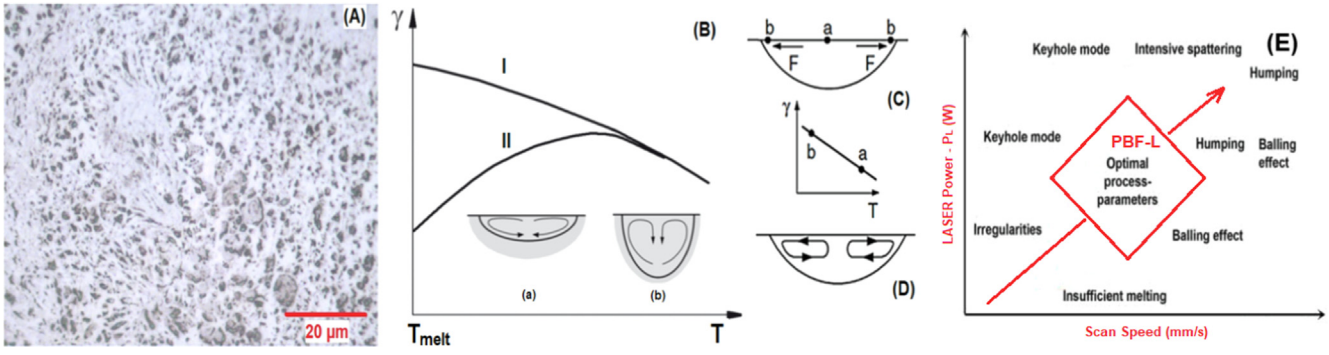

Fig. 9. (A) Microstructure of W-30Ni Alloy Sample 3; PL = 100 W, vs = 50 mm/s and Ev = 417 J/mm^3. (B) Schematic figure of the Marangoni effect, Surface tension (γ) × temperature (T). (C and D) Influence of surface tension force on the convection mode in the molten pool [12] and (E) schematic diagram of an optimal PBF-L process parameter window.

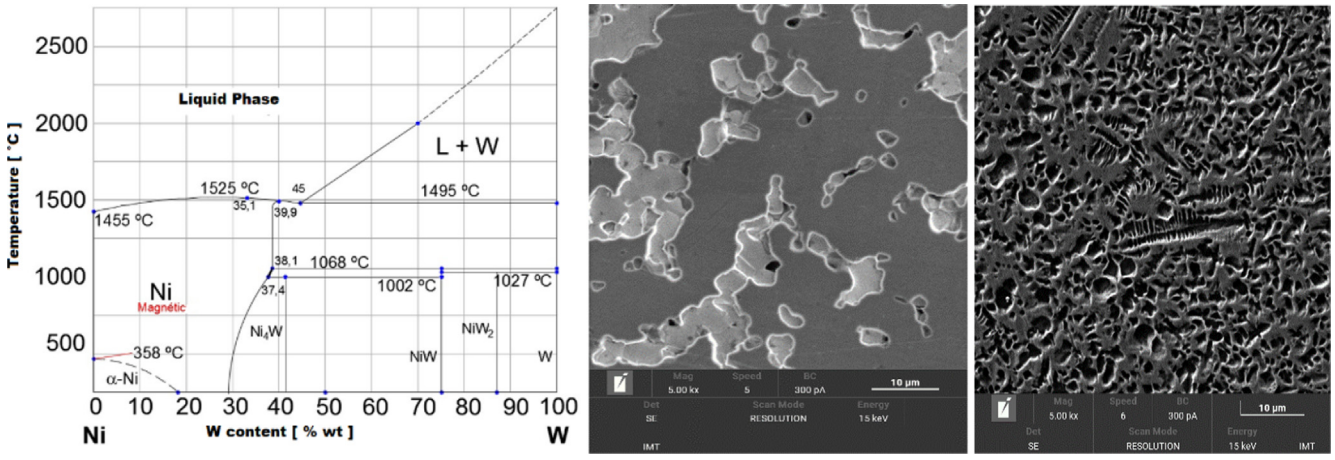

Fig. 10. (A) W-Ni phase diagram, (B) SEM of the vacuum sintered sample at 1420 °C, binding of W-solid grains - W-solid. (C) SEM of sample III sintered via PBF-L.

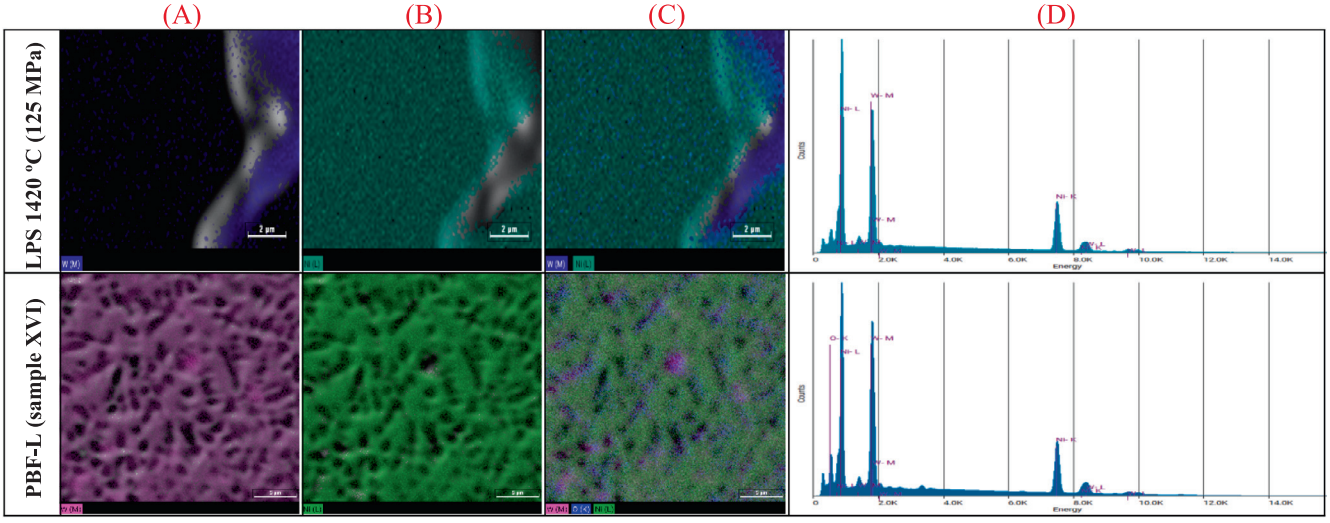

Fig. 11. SEM EDS analysis (10,000x) Element Images of W-Ni alloy, comparison of microstructures processed by LPS (1420 °C, 125 MPa) and PBF-L techniques (sample XVI), (A) highlight for the particle W, (B) highlight for the Ni-binding phase and (C) distribution of solute W in the Ni-solvent binding phase e (D) energy-dispersive X-ray spectroscopy for chemical characterization of the samples.

in the system. Understanding the critical material (powder type) and process parameters (laser power, distance between tracks, layer thickness, scan speed affect PBF-L processing for W alloys [16]. For mapping power parameters (W) as a function of the scanning speed (mm/s), in the PBF-L technique and for the other techniques of additive manufacturing in metals, evidence other important characteristics such as the melting points of chemical elements, the presence of unwanted effects such as keyhole, humping, balling, spattering and lack of fusion, illustrated in Fig. 9 (E).

In the W-30Ni alloy, obtained by the conventional LPS route, the dominant phase should be the solid solution of W in Ni, as indicated by the W-Ni equilibrium diagram, Fig. 10 (A). However, the structures obtained by the PBF-L technique may differ significantly from those obtained by thermal equilibrium, that is, a complex process, in which the samples are out of equilibrium, and isolated intermetallic compounds may appear of NiW_2 and Ni_4W, with the NiW phase in greater proportion, but difficult to be identified in OM and SEM microscopes. Alternative compositions for WHA's can be easily designed for specific applications. What should be avoided are the brittle intermetallic precipitations for alloys with Ni-rich binders, as they can form the Ni_4W phase in slow cooling, and its elimination is possible by a post-intermediate heat treatment. In liquid phase sintering, W dissolves in the metal matrix Ni (FCC), with 20–25% by weight, being precipitated on cooling to room temperature [17]. However, it does not indicate whether one of these phases, mentioned above, at elevated temperatures, can be kept at room temperature by rapid cooling. For some parameters of the PBF-L technique, they indicated good homogeneity attributable to the solid solution of W in Ni, unlike the conventional LPS technique, which showed heterogeneous structures for different temperatures [15]. Having a well-spheroidized microstructure in shielding components for ionizing radiation is especially important from the point of view of durability [5]. Phase diagrams do not indicate the phases produced by fast cooling rates. The W-Ni phase diagram has limitations, it only provides information on the constitution of the alloys, for example the number of phases (NiW or NiW_2) present for the chemical composition 70W-30Ni but does not provide information on the structural distribution of the phases; that is, they do not indicate the particulate size, shape or phase distribution, which affects the final mechanical properties [15].

An important observation in the W-Ni alloy, processed by PBF-L, Fig. 10 (C), about the change in the morphology of the W particu-

lates, compared to LPS, Fig. 10 (B), indicates that the surface energy of the W-Ni particulates accelerated the diffusion process accentuated W, intensifying the mass transfer to the binding phase, Fig. 11 (A), (B) and (C), changing the composition and contributing to the binder phase hardening. In WHA alloys, via SEM, three main regions are evidenced in the microstructure: the W particulate phase, the metallic matrix or binding phase and a region of dendritic formation for W-Ni alloy. W has a high solubility in the Ni matrix, but the solubility of Ni in W is practically negligible, Fig. 11. Furthermore, fine W dendrites that formed in the matrix (PBF-L), when W particles are partially diffused, on rapid cooling, W particles acted as heterogeneous nucleation sites [18]**.** For high direct sintering energies, the presence of oxygen in the spectrum of sample XVI, is noted (P_L 125W, v_s 125 mm/s and E_V 333 J/mm^3), allowing the possible formation of WO_3, Fig. 11 (D), EDS characterization of the samples PBF-L.

4. Conclusions

In this work, the behavior of the heavy metal alloy W-30Ni, with irregular particles and poor flowability, was sintered directly (PBF-L) and indirectly (LPS). There is no published literature, considering the same chemical composition, i.e., The conclusions are given below:

I. In the LPS technique, with increasing sintering temperature, the relative density and microhardness of the samples increased. With increasing compaction pressure, linear and volumetric shrinkage decreased. The best relative density reached about 92% for a temperature of 1420 °C. Regarding the microstructure, solid sintering of the W-W particulates occurs, obtaining a heterogeneous structure with micro porosities. The sintering temperature for the W-30Ni alloy should continue above 1420 °C for better densification, porosity reduction and to improve the distribution of W particulates in the Ni binder phase. The hardness of the W-30Ni samples were higher than the WHA alloys (10% wt. Ni) described in the literature.

II. Tungsten Heavy Alloy alloy with high binder content, for 30wt.%Ni. This composition is not covered by the ASTM B777 standard, with a maximum binder content of 10 wt%. We are using such high amount of binder to investigate the liquid phase, especially during PBF-L processes. For the PBF-L technique, the microhardness test (HV) resulted in higher values than the PM-LPS technique, due to the diffusion and precipitation of W in the binding phase and the formation of intermetallic compounds (NiW_2, Ni_4W and NiW) is an important reason for the change in the hardness behavior of the W-30Ni alloy, reaching a minimum of 508 $HV_{0.5}$ and a maximum of 612 $HV_{0.5}$. For energies above 300 J/mm^3, the microstructures showed good homogeneity attributable to the solid W in Ni solution. However, in the presence of oxygen. The relative density of the PBF-L samples was not investigated, due to the very thin sample thickness. No microcracks were evidenced in the W-30Ni samples, this is important to see if the PBF-L technology is viable and if it is ready to proceed to the process of developing W-30Ni alloy products for free geometries. However, there was a lack of fusion for samples with energies below 300 J/mm^3. For this W-30Ni alloy, proceed above 125 W to reduce the apparent porosity.

CRediT authorship contribution statement

F. Miranda: Conceptualization, Data curation, Formal analysis, Investigation, Methodology, Visualization, Writing - original draft. **D. Rodrigues:** Funding acquisition, Project administration, Resources, Validation, Writing - review & editing.

Data availability

Data will be made available on request.

Declaration of Competing Interest

The authors declare that they have no known competing financial interests or personal relationships that could have appeared to influence the work reported in this paper.

Acknowledgements

The authors acknowledge Brats Filters and Metal Powders, Omnitek Technology and the Maua Institute of Technology for the partnerships and São Paulo Research Foundation (FAPESP), for the support grants 22/06201-7.

References

[1] D. Wang, C. Yu, X. Zhou, J. Ma, W. Liu, Z. Shen, Dense pure tungsten fabricated by selective laser melting, Appl. Sci. 7 (2017) 430, https://doi.org/10.3390/app7040430.
[2] J. Chaurasia, M. Ayyapan, P. Patel, R. Annamalai, A. Rajan, Activated sintering of tungsten heavy alloy, Sci. Sinter. 49 (2017), https://doi.org/10.2298/SOS1704445C.
[3] N.B. Erhardt, P. Suri, R.M. German, Microstructural evolution of W-Ni-Fe during liquid phase sintering – a quenching study, Center Innov. Sint. Prod. 147 (2003) 16802–16809.
[4] K. Lee, S. Cha, H.J. Ryu, S. Hong, Effect of two-stage sintering process on microstructure and mechanical properties of ODS tungsten heavy alloy, Mater. Sci. Eng. A-Struct. Mater. Proper. Microstruct. Process. 458 (2007) 323–329, https://doi.org/10.1016/j.msea.2007.01.118.
[5] S.G. Caldwell, A Review of Tungsten Heavy Alloy Utilization in Isotope Transport Containers. WM2013 Conference, February 24th–28th, 2013, Phoenix, Arizona USA. <http://archive.wmsym.org/2013/papers/13380.pdf>.
[6] A. Sidambe, Y. Tian, P. Prangnell, P. Fox, Effect of processing parameters on the densification, microstructure, and crystallographic texture during the laser powder bed fusion of pure tungsten, Int. J. Refract. Metals Hard Mater. 78 (2018), https://doi.org/10.1016/j.ijrmhm.2018.10.004.
[7] A. Budding, T. Vaneker, New strategies for powder compaction in powder-based rapid prototyping techniques, Proc. CIRP. 6 (2013) 528–533, https://doi.org/10.1016/j.procir.2013.03.100.
[8] E. Uhlmann, A. Bergmann, W. Gridin, Investigation on additive manufacturing of tungsten carbide-cobalt by selective laser melting, Proc. CIRP. 35 (2015) 8–15, https://doi.org/10.1016/j.procir.2015.08.060.
[9] T. Niino, K. Sato, Effect of powder compaction in plastic laser sintering fabrication, in: 20th Annual International Solid Freeform Fabrication Symposium, SFF, 2009.
[10] J. Li, Y. Wu, B. Zhou, Z. Wei, Laser powder bed fusion of pure tungsten: effects of process parameters on morphology, densification, microstructure, Materials 14 (2021) 165, https://doi.org/10.3390/ma14010165.
[11] R.M. German, P. Suri, S.J. Park, Review: liquid phase sintering, J. Mater. Sci. 44 (2009) 1–39.
[12] S. Kou, Welding Metallurgy, John Wiley & Sons Inc, Hoboken, NJ, USA, 2002.
[13] T. Debroy, H. Wei, J. Zuback, T. Mukherjee, J. Elmer, J.O. Milewski, A. Beese, A. Wilson-Heid, A. De, W. Zhang, Additive manufacturing of metallic components – process, structure and properties, Prog. Mater. Sci. 92 (2018) 112–224, https://doi.org/10.1016/j.pmatsci.2017.10.001.
[14] ASM Handbook, Alloy Phase Diagrams, V.3 ASM International, 1992. ISBN:087170377-7.
[15] F.C. Campbell, Phase diagrams - understanding the basics, ASM Int. Chapter 14 (2012) 291–301.
[16] R. Enneti, R. Morgan, T. Wolfe, A. Harooni, S. Volk, Direct metal laser sintering (DMLS) of Tungsten powders, Int. J. Powder Metall. 53 (4) (2017) pp.
[17] N. Serkhane-Ouabadi, G. Benalia-Baguenane, M. Nechiche, S. Azemu, Influence of the liquid phase and the carbon on the reactive sintering in mixtures W-Ni-C, U.P.B. Sci. Bull., Series B 84 (1) (2022), ISSN 1454-2331.
[18] J. Li, Z. Wei, B. Zhou, Y. Wu, S.-G. Chen, Z. Sun, Densification, microstructure and properties of 90W–7Ni-3Fe fabricated by selective laser melting, Metals 9 (2019) 884.